

Distinguishing Phases with Ansatz Wavefunctions

B. Bauer and M. Troyer

Theoretische Physik, ETH Zurich, 8093 Zurich, Switzerland

V.W. Scarola*

*Theoretische Physik, ETH Zurich, 8093 Zurich, Switzerland and
Department of Chemistry and Pitzer Center for Theoretical Chemistry,
University of California, Berkeley, California 94720, USA*

K.B. Whaley

*Department of Chemistry and Pitzer Center for Theoretical Chemistry,
University of California, Berkeley, California 94720, USA*

(Dated: June 5, 2018)

We propose an indistinguishability measure for assessment of ansatz wavefunctions with numerically determined wavefunctions. The measure efficiently compares all correlation functions of two states and can therefore be used to distinguish phases by defining correlator classes for ansatz wavefunctions. It also allows identification of quantum critical points. We demonstrate the approach for the transverse Ising and bilinear-biquadratic Heisenberg models, using the matrix product state formalism with the time evolving block decimation algorithm.

PACS numbers: 02.70.-c, 03.67.-a, 05.70.Jk, 05.70.Jk

I. INTRODUCTION

A growing number of quantum many-body models have been constructed to study order that is readily characterized by wavefunctions as opposed to simple order parameters. Models of topological order¹ in particular can be examined with a combination of numerical techniques and ansatz states. Examples include idealized models of the fractional quantum Hall regime^{2,3,4} and spin liquids such as the AKLT model⁵ or the toric code⁶. The exact ground states of these models, e.g., the Laughlin⁷ or valence bond solid⁵ (VBS) wavefunctions, serve as ansatz states for more realistic many-body models. A comparison of idealized ansatz wavefunctions and numerically obtained, realistic wavefunctions then becomes an essential element in the search for novel phases in real materials.

Several procedures are currently available for verifying ansatz states. The variational theorem allows comparison of the energetics of proposed ground states. It is useful in ruling out trial states but can fail in establishing a particular trial state because irrelevant wavefunctions often show competitive energetics. Diagonalization of small systems can be used to compute overlaps between ansatz and exact states. But the scaling of overlap to larger systems does not always allow for a clear identification of a particular phase. For example diagonalization studies⁸ of proposed $\nu = 5/2$ fractional quantum Hall states show overlaps of $\sim 0.8 - 0.9$ of competing paired states, complicating unambiguous identification of the true ground state. Variational tests and overlaps must be combined with systematic analyses of other correlation functions to make a case for how well an ansatz state captures output from numerics.

In the following, we present a new measure for assessment of ansatz wavefunctions by comparison with numer-

ical wavefunctions that allows for a clear identification of a particular phase. This measure, which we refer to as the indistinguishability, I , is based on a quantum information measure of quantum state distinguishability^{9,10,11}. We demonstrate the use of this indistinguishability measure by application to the assessment of ansatz wavefunctions for the ground state of two different models, the transverse Ising chain and the spin-one bilinear-biquadratic Heisenberg chain. The former provides a simple test of the approach while the latter allows us to exploit its power to analyze a challenging and rich model whose solution has not yet been fully characterized. We use accurate ground state wavefunctions that are obtained with the time-evolving block decimation algorithm of Vidal^{12,13}. This yields the state in the form of a matrix-product state (MPS)^{14,15}, from which our measure can easily be calculated. We note that the notion of quantum state distinguishability has been used recently to derive order parameters¹⁶. We emphasize that we take an entirely different approach here by using distinguishability to assess the degree of similarity of a proposed ansatz wavefunction with output from an accurate simulation, thereby gaining insight from the structure of the wavefunctions.

We also show that the indistinguishability measure allows identification of quantum critical points and leads to an indistinguishability susceptibility that provides an accurate signature of these. Recent work has explored the characterization of quantum phase transitions without making recourse to ansatz wavefunctions. Instead, quantities related to quantum information theory such as concurrence^{17,18}, entanglement entropy¹⁹ and fidelity^{20,21} have been used to extract information about quantum phase transitions from numerical output. These and other quantities signal changes of phase but without

revealing detailed information about the nature of the quantum states.

The outline of this paper is as follows: in Sect. II and III, we introduce the new measure and discuss the scaling in the thermodynamic limit. In Sect. IV, we show how to calculate the measure efficiently for a given state in the MPS representation. In Sect. V and VI, we discuss our results for the transverse Ising chain and the bilinear-biquadratic Heisenberg chain, respectively.

II. INDISTINGUISHABILITY

We define the indistinguishability $I_n(A,E)$ of two N -particle states, an ansatz state Ψ_A and the exact state Ψ_E , as the n -particle probability of error in distinguishing the two states with an n -particle measurement:

$$I_n(A,E) = \frac{1}{2} - \frac{1}{4} \text{Tr} |\rho_E^{(n)} - \rho_A^{(n)}| \quad (1)$$

where $\text{Tr}|\mathcal{O}|$ is the trace norm of \mathcal{O} and $\rho^{(n)} = \text{Tr}_{N-n}(\rho)$ is the n -particle reduced density matrix^{9,10,11}. The last term in Eq. 1 is a well known statistical distance measure, the Kolmogorov distance between two probability distributions. When $I_n(A,E)$ is zero, the states are distinguishable and the ansatz wavefunction Ψ_A is clearly a bad approximation to Ψ_E . However, when it is non-zero, there is a finite probability that an n -particle measurement can not distinguish the ansatz from the numerical wavefunction, implying that the ansatz provides a good description of the state up to n -particle correlators. $I_n(A,E) = 1/2$ corresponds to maximum indistinguishability, implying identical states. Since the measure is defined in terms of reduced density matrices, the state indistinguishability implicitly scans all correlators with up to n particles, to yield a single number that quantifies the ability of an optimally chosen set of n -particle correlators to distinguish two states^{9,10}. $1 - I_n$ gives the probability that an optimally chosen correlation function involving at most n particles will be able to distinguish the two states.

We use I_n as a quantifier of the degree of *indistinguishability* of two states via correlators in an N -particle system. When I_n is intensive in N , so that small n values suffice to characterize the correlators, we define two states to be in the same n -particle *correlator class* if I_n is finite in the thermodynamic limit, i.e., as $N \rightarrow \infty$, and to be in different correlator classes if $I_n = 0$ in this limit.

III. QUANTUM CHERNOFF BOUND

It is possible that I_n vanishes in the thermodynamic limit regardless of the ansatz. When I_n is extensive in N so that large n values are required (e.g., $n \sim \mathcal{O}(N)$), we can nevertheless use the scaling of I_n with N to identify correlator classes. The scaling of the indistinguishability

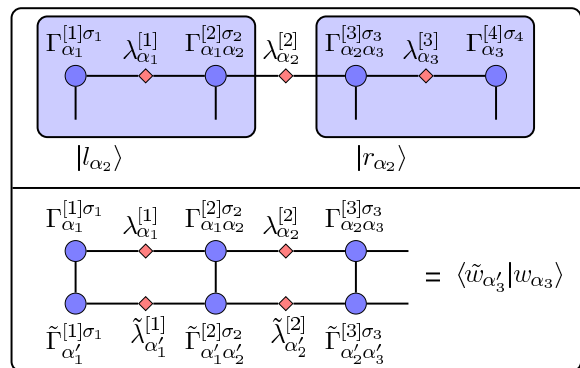


Figure 1: Top: Schematic of the matrix product decomposition of a four-site lattice. The circles indicate sites, i , with an applied tensor, $\Gamma^{[i]}$, and the diamonds denote bonds which carry Schmidt coefficients, $\lambda^{[i]}$, on the i^{th} bond. The shading indicates a decomposition into left and right subsystems described by a renormalized basis $|l_\alpha\rangle$ and $|r_\alpha\rangle$ of eigenvectors of the respective reduced density matrices. Bottom: Schematic depicting an overlap of two matrix product states. The top line corresponds to a state A (e.g., an ansatz state) in the matrix product representation while the bottom line corresponds to a second state E (e.g., an exact state).

bility to the thermodynamic limit can be quantified in terms of the quantum Chernoff bound (QCB). Assuming that on sufficiently large scales, a translationally invariant ground state can be regarded as a tensor product of subblocks (or copies), a recent result²² for the indistinguishability of many copies of the system shows that we should expect an exponential dependence for large n , i.e.: $I_n \sim \exp(-n\xi_{\text{CB}})$, where the QCB can be identified in the thermodynamic limit from

$$\xi_{\text{CB}}^{\text{lim}} = - \lim_{n \rightarrow \infty} \log(I_n)/n \quad (2)$$

with $n = N/2$. A remarkable relation²² connects the QCB directly to the reduced density matrices of *finite* blocks, namely

$$\xi_{\text{CB}}^{\text{lim}} \equiv \xi_{\text{CB}}^\rho \quad (3)$$

with

$$\xi_{\text{CB}}^\rho = - \log \min_{0 \leq s \leq 1} \text{Tr} \left[(\rho_A^{(n)})^s (\rho_E^{(n)})^{1-s} \right], \quad (4)$$

thereby allowing a direct evaluation in terms of the reduced density matrices $\rho_E^{(n)}$ and $\rho_A^{(n)}$. Using either of these expressions for the QCB we can then identify correlator classes in the thermodynamic limit: small values of ξ_{CB} correspond to large values of I_n and indicate a successful ansatz.

IV. CALCULATING I USING MATRIX-PRODUCT STATES

Our simulation uses an MPS approximation to a state in the full spin Hilbert space. The coefficients $c(\{\sigma_i\})$ of the expansion of the state in the σ^z -basis,

$$|\Psi\rangle = \sum_{\{\sigma_i\}} c(\{\sigma_i\}) |\sigma_1\rangle \dots |\sigma_N\rangle \quad (5)$$

are given as a product of matrices:

$$c(\{\sigma_i\}) = \sum_{\alpha_1, \dots, \alpha_N} \Gamma_{\alpha_1}^{[1]\sigma_1} \lambda_{\alpha_1}^{[1]} \Gamma_{\alpha_1 \alpha_2}^{[2]\sigma_2} \lambda_{\alpha_2}^{[2]} \dots \Gamma_{\alpha_N}^{[N]\sigma_N}, \quad (6)$$

where α indexes the auxiliary state space (of size M), Γ are rank three tensors that must be determined, and the coefficients λ are the Schmidt eigenvalues of a bipartite splitting of the system at that site, i.e. they are equal to the eigenvalues of the reduced density matrices obtained by such a splitting. In the following we denote MPS states as $|\Psi\rangle = (\Gamma_{\alpha_i \beta_i}^{[i]\sigma_i}, \lambda_{\beta_i}^{[i]})$.

The accuracy of the MPS approximation depends on the decay of these eigenvalues and can be controlled by tuning the matrix dimension M . In the case of the Ising model in transverse field, the Schmidt coefficients are found to decay very quickly. We therefore perform our calculations with a matrix size $M = 100$ and up to $N = 64$ spins. Imaginary time evolution is used to project into the ground state. We apply a first-order Trotter decomposition with an initial time-step $d\tau = 0.05$, which is decreased to $d\tau = 0.0001$ during the simulation. In what follows an "exact" state (E) refers to an MPS approximation to the exact ground state.

Once the ground state has been found, we must obtain the density matrix in a common, orthonormal basis $\{|v_a\rangle\}$ for both the ansatz and exact states. We first join the two bases by concatenating Schmidt coefficients and the tensors blockwise, i.e. for two states $|\Psi\rangle = (\Gamma_{\alpha_i \beta_i}^{[i]\sigma_i}, \lambda_{\beta_i}^{[i]})$, $|\tilde{\Psi}\rangle = (\tilde{\Gamma}_{\alpha_i \beta_i}^{[i]\sigma_i}, \tilde{\lambda}_{\beta_i}^{[i]})$ we have $|\hat{\Psi}\rangle$ given by

$$\hat{\Gamma}_{\alpha\beta}^{[i]\sigma} = \begin{cases} \Gamma_{\alpha\beta}^{[i]\sigma} & \alpha, \beta \in \{1, \dots, M\} \\ \tilde{\Gamma}_{\alpha\beta}^{[i]\sigma} & \alpha, \beta \in \{M+1, \dots, 2M\} \end{cases} \quad (7)$$

$$\hat{\lambda}_{\alpha}^{[i]} = \begin{cases} \lambda_{\alpha}^{[i]} & \alpha \in \{1, \dots, M\} \\ \tilde{\lambda}_{\alpha}^{[i]} & \alpha \in \{M+1, \dots, 2M\}. \end{cases} \quad (8)$$

We define the overlap matrix of two sets of states $|w_m\rangle = (\Gamma_{\alpha\beta}^{[i]\sigma_i}, \lambda_{\beta}^{[i]})$ and $|\tilde{w}_m\rangle = (\tilde{\Gamma}_{\alpha\beta}^{[i]\sigma_i}, \tilde{\lambda}_{\beta}^{[i]})$ describing some part of the system (bottom panel, Fig. 1), which are taken to be the Schmidt eigenvectors of a bipartite decomposition of the system:

$$\langle \tilde{w}_{\alpha'_n} | w_{\alpha_n} \rangle = \sum_{\mathcal{F}} \left(\overline{\prod_i \tilde{\Gamma}_{\alpha'_i \alpha'_i}^{[i]\sigma_i} \tilde{\lambda}_{\alpha'_i}^{[i]}} \prod_i \Gamma_{\alpha_i \alpha_i}^{[i]\sigma_i} \lambda_{\alpha_i}^{[i]} \right), \quad (9)$$

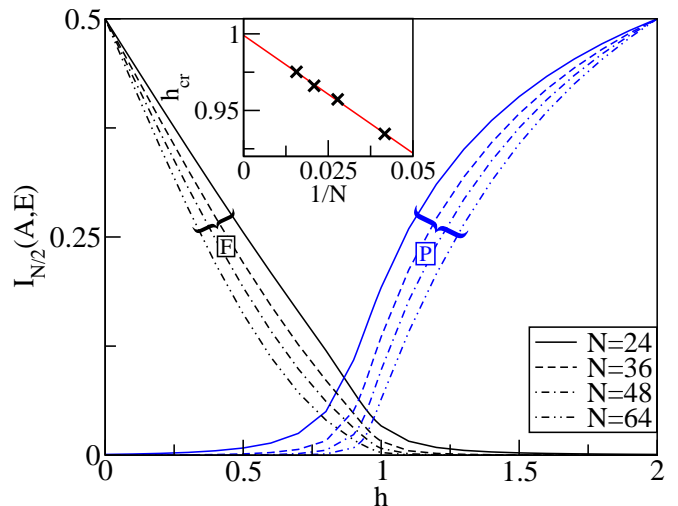


Figure 2: (color online) Indistinguishability $I_{N/2}(A, E)$ plotted as a function of magnetic field h for the one-dimensional transverse quantum Ising model for several different system sizes, N , and two different ansatz states, $A = F$, (ferromagnetic, $h_{\text{ref}} = 0$, black lines) and $A = P$ (paramagnetic, $h_{\text{ref}} = 2$, blue lines). The inset plots the crossing point of $I_{N/2}(F, E)$ and $I_{N/2}(P, E)$, with Ψ_P evaluated for $h_{\text{ref}} = 100$, versus N^{-1} . A straight line fit yields a quantum critical point at $h_{\text{cr}} = 0.999(1)$ as $N \rightarrow \infty$, in agreement with standard results²³.

where the summation runs over all orthogonal spin configurations and \mathcal{F} indicates the summation over all remaining indices. This allows us to find a transformation that we can use to orthonormalize the basis of $|\hat{\Psi}\rangle$ for a specific bipartition.

The reduced density matrices can now be computed using

$$\rho_{a,b}^{\text{red}} = \sum_{\alpha, \beta, t} \lambda_{\alpha} \lambda_{\beta} \langle v_a | l_{\alpha} \rangle \langle l_{\beta} | v_b \rangle \langle r_t | r_{\alpha} \rangle \langle r_{\beta} | r_t \rangle. \quad (10)$$

$|r_{\alpha}\rangle$ and $|l_{\alpha}\rangle$ denote states obtained from a right and left partitioning of the lattice (top panel, Fig. 1). The sum over states $|r_t\rangle$ traces out the right $N - n$ sites.

V. ISING CHAIN IN TRANSVERSE FIELD

We first apply the indistinguishability measure to the simplest model with a quantum phase transition, the ferromagnetic transverse Ising model:

$$H_{\text{Is}} = - \sum_i \sigma_i^x \sigma_{i+1}^x - h \sum_i \sigma_i^z. \quad (11)$$

Here σ_i^{α} , $\alpha = x, y, z$ are the Pauli matrices and the sites i are located on an N -site chain with open boundary conditions. For a review of the properties of this model see Ref. (23) and references therein.

Physically motivated ansatz wavefunctions can be de-

finer for Eq. (11) by noting that for $h > 1$ the ground state is a paramagnet with exponentially decaying correlators, $\langle \sigma_0^x \sigma_j^x \rangle \sim \exp(-j/\xi)$, while for $h < 1$ the ground state is in the ferromagnetically ordered phase with long range order, $\langle \sigma_0^x \sigma_j^x \rangle \sim m^2$ for $j \rightarrow \infty$, where m is the spontaneous magnetization. On the ferromagnetic side the exact $h \rightarrow 0$ ground state (one of the two degenerate ground states) is given by: $\Psi_F = \prod_i |\uparrow\rangle_i$, while on the paramagnetic side in the limit $h \rightarrow \infty$ we have: $\Psi_P = \prod_i |\rightarrow\rangle_i$. These states are ansatz wavefunctions that we will apply at all values of magnetic field h . In the thermodynamic limit there is a quantum phase transition at $h = 1$. Without relying on the explicit behavior of any correlation functions, we will show using I_n that for $h \neq 1$ our ansatz wavefunctions fall into two distinct correlator classes that characterize the two phases on either side of the transition. I_n thus allows an efficient test of the accuracy of ansatz states in reproducing all n -particle correlation functions of the exact state, without explicit calculation of these. We further show that the location of the transition can be accurately identified.

We focus here on calculations for large values of n that will allow us to analyze the scaling of I_n when this is an intensive quantity. Thus we consider $n = N/2$, where the total number of spins N varies. The indistinguishability $I_{n=N/2}$ of the exact ground state of Eq. (11) with the ferromagnetic and paramagnetic ansatz states Ψ_F and Ψ_P was computed. We use $\Psi_F = \Psi_E^{h_{\text{ref}}=0}$ for the ferromagnetic ansatz. For most calculations it is sufficient to use $\Psi_P = \Psi_E^{h_{\text{ref}}}$ with $h_{\text{ref}} = 2$ for the paramagnetic ansatz but larger values of h_{ref} will be used to extract information about the phase transition.

The calculated indistinguishabilities $I_{N/2}(F, E)$ and $I_{N/2}(P, E)$ are shown in the main panel of Fig. 2 as a function of h for several system sizes. For $h \lesssim 1$, we find $I_{N/2}(F, E)$ large with a weak decay with N . In contrast, we find here a strong suppression of $I_{N/2}(P, E)$ as $N \rightarrow \infty$, implying that an optimally chosen correlator of up to $N/2$ particles will not successfully distinguish the exact state from Ψ_F but will successfully distinguish the exact state from the paramagnetic state for large enough N . For $h \gtrsim 1$, we find the reverse situation.

We can use I_n to accurately identify the phase transition point, h_{cr} . We search for the critical point by finding the h at which $I_{N/2}(F, E) = I_{N/2}(P, E)$ and extrapolating to the thermodynamic limit. The inset of Fig. 2 shows a linear extrapolation in $1/N$ that agrees with the known solution, $h_{\text{cr}} = 1$.

We compute the QCB for each of the two phases in the transverse Ising model to demonstrate that the existence of two distinct correlator classes can also be found via the scaling exponent of I_n . Fig. 3 plots the QCB versus h evaluated with two different methods. The dotted lines plot the finite size extrapolation of $\xi_{\text{CB}}^{\text{lim}}$ for both A=F ($h_{\text{ref}} = 0$, black) and A=P ($h_{\text{ref}} = 2$, blue). The remaining lines show how the data collapse towards this line for several discrete N values. We see that the scaling exponent, ξ_{CB} , remains finite in the thermodynamic limit and

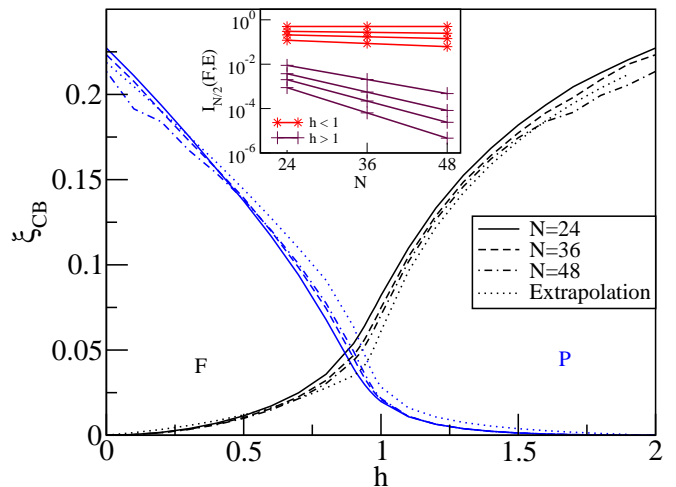


Figure 3: (color online) The quantum Chernoff bound versus magnetic field using the extrapolation of indistinguishability, $\xi_{\text{CB}}^{\text{lim}}$, (dotted line) and the reduced density matrices directly, $\xi_{\text{CB}}^{\text{P}}$, (solid, dashed and dot-dashed). A suppression of ξ_{CB} indicates success for the ferromagnetic, F, black lines (paramagnetic, P blue lines) ansatz for $h \lesssim 1$ ($h \gtrsim 1$). The inset plots shows a log plot of $I_{N/2}(F, E)$ versus N for several h to show an abrupt change in scaling near $h = 1$.

correctly identifies correlator classes on either side of the critical point. Precise location of the critical point from the QCB is complicated by the need to extrapolate an exponent and the associated numerical error. Location from the scaling of I_n as in Fig. 2 is more direct and appears more robust in this case.

The critical point can be defined in terms of the indistinguishability as the unique point in parameter space that, for a given ansatz wavefunction, separates regions characterized by dramatically different scaling of I_n . As demonstrated above, both the direct evaluation of I_n and evaluation of the QCB allow the critical point between two phases to be located as the point where the indistinguishability measures for the two different ansatz functions are equal. To further characterize the critical point for finite sized systems we can define an indistinguishability susceptibility for $I_n(A, E)$ by

$$\begin{aligned} \chi_{I_n} &= \lim_{h \rightarrow \pm h_{\text{ref}}} dI_n(\Psi_E^{h_{\text{ref}}}, \Psi_E^h) / dh \\ &= \lim_{\varepsilon \rightarrow 0} \frac{0.5 - I_n(\Psi_E^{h_{\text{ref}}}, \Psi_E^{h_{\text{ref}} \pm \varepsilon})}{\pm \varepsilon} \end{aligned} \quad (12)$$

where we have used $\Psi_A = \Psi_E^{h_{\text{ref}}}$. Eq. (12) should coincide with the maximum of the derivative of $I_n(A, E)$ for a given h_{ref} , when $\Psi_A = \Psi_E^{h_{\text{ref}}}$. Our direct calculations of I_n show that for the transverse Ising model, the critical point can be identified with a peak in $\chi_{I_{N/2}}$ versus h .

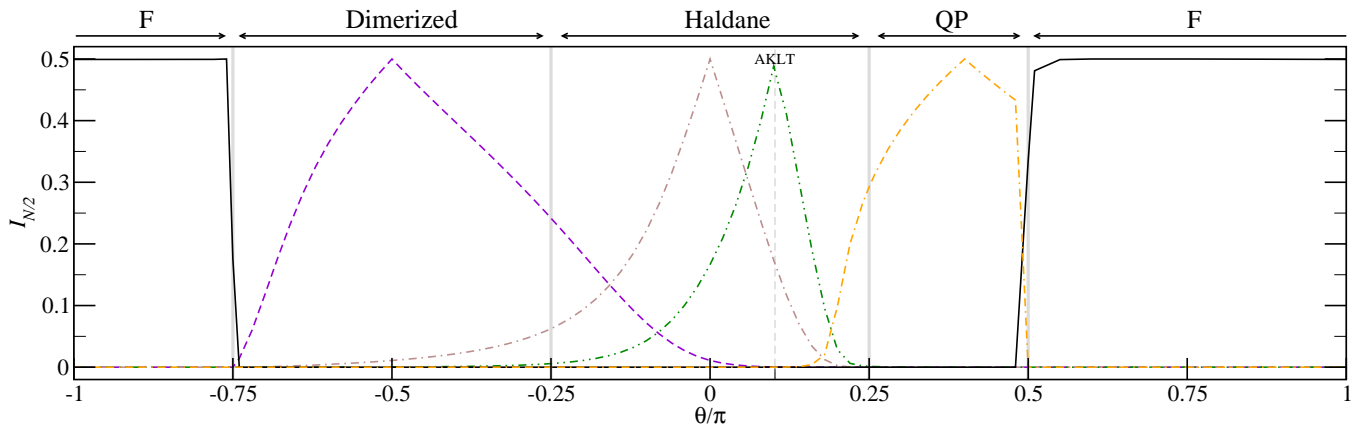


Figure 4: Indistinguishability versus θ for the bilinear-biquadratic Heisenberg model, Eq. 13, with $N = 36$ and $n = 18$. Distinct correlator classes surround 5 different reference states for which $I_{N/2} = 1/2$: the ferromagnetic (solid), quadrupolar (dot-double dashed), Haldane (dot-dashed) and dimerized (dashed) phases. The AKLT point (double dot-dashed) at $\theta = \tan^{-1}(1/3)$ appears within the Haldane phase.

VI. SPIN-1 BILINEAR-BIQUADRATIC CHAIN

We now apply our distinguishability measure to analyze a richer model with ground states characterized by more complicated correlators, the bilinear-biquadratic Heisenberg chain, defined by

$$H_{\text{bl-bq}} = \sum_i [\cos \theta (\mathbf{S}_i \mathbf{S}_{i+1}) + \sin \theta (\mathbf{S}_i \mathbf{S}_{i+1})^2], \quad (13)$$

where \mathbf{S} is the spin-1 operator and θ a parameter. A growing body of analytic and numerical work has shown that this model hosts a variety of ground state phases (for a review see Ref. (24) and references therein).

An integrable point^{5,25} at $\theta_{\text{AKLT}} = \tan^{-1} 1/3$ has a particularly simple form for the exact ground state that belongs to a class of VBS wavefunctions related to the Laughlin ansatz state²⁶. The VBS state at θ_{AKLT} can be written as $\Psi_{\text{VBS}} = \prod_i (a_i^\dagger b_{i+1}^\dagger - b_i^\dagger a_{i+1}^\dagger) |0\rangle$, where a and b annihilate Schwinger bosons defined by $S^x + iS^y = a^\dagger b$, $S^z = (a^\dagger a - b^\dagger b)/2$, and $a^\dagger a + b^\dagger b = 2$. Ψ_{VBS} characterizes a state with exponentially decaying local correlators. The AKLT state is also characterized by hidden, long-ranged chain correlators²⁷. Notably, this state does not break translational symmetry. On a finite chain with open boundary conditions, a four-fold degeneracy appears which is related to open spin-1/2 degrees of freedom at the ends of the chain.

We address the phases of this model from the point of view of ansatz states by taking five specific values of θ as reference points to capture the various possible phases. In particular, we choose $\theta_{\text{ref}} = \pi$ for the ferromagnetic (F) phase, $\theta_{\text{ref}} = 0.4\pi$ for the quadrupolar (QP) phase, $\theta_{\text{ref}} = 0$ and $\theta_{\text{ref}} = \theta_{\text{AKLT}}$ for the Haldane phase (corresponding to the Heisenberg and AKLT states) and $\theta_{\text{ref}} = -\pi/2$ for the dimerized phase. In addition to these ansatzes defined by the ground states of the Hamiltonian Eq. (13) for the five reference θ values, we shall also con-

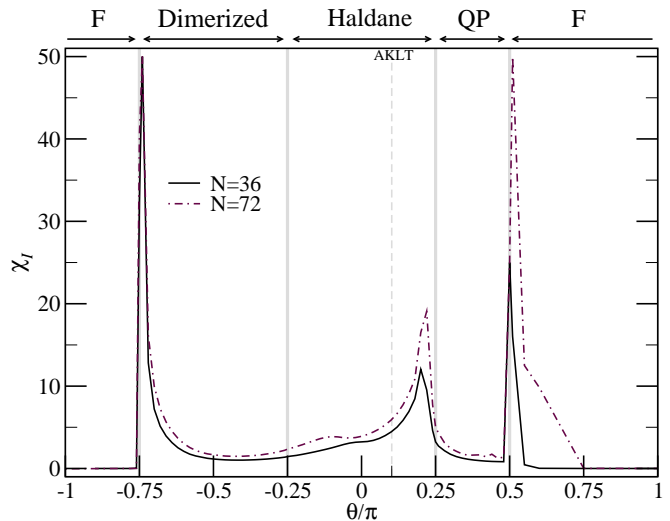


Figure 5: Indistinguishability susceptibility, Eq. 12, computed for the bilinear-biquadratic chain, Eq. 13. Here we use $N = 36, 72$, $n = N/2$ and $\varepsilon = 0.02$ for the relevant part of the phase diagram. The peaks indicate phase transitions. In the case of discontinuous transitions, peaks remain finite only due to the discretization of the values of h_{ref} .

sider a trial wave function for a fully dimerized state, obtained at $\theta = -\pi/2$ with a modified Hamiltonian that results from omitting all even-bond terms in Eq. (13).

Since, with the exception of the Haldane phase, analytic forms for the ground state wave function at these reference points are not known, the ansatz wavefunctions are given here by numerical solution for the ground state of Eq. (13) at the reference values of θ_{ref} . These numerical solutions Ψ_A are generated with the matrix product approach of Section IV at θ_{ref} , just as the exact solutions Ψ_E are generated at arbitrary values of θ . This illustrates

an important practical feature of the method, namely that we are not restricted to use of analytic ansatz functions. We then calculate the indistinguishability measure, $I_{N/2}$, for system sizes $N = 24 \dots 72$ with open boundary conditions. Due to this choice of boundary conditions, we need to take N as a multiple of 3 in order to be able to capture correlations at $k = 2\pi/3$ which are important in the quadrupolar phase.

A typical result, for $N = 36$, is presented in Fig. 4, which shows $I_{N/2}$ as a function of θ for the five different correlator classes defined by the above values of θ_{ref} . The general variation of $I_{N/2}$ for each correlator class is consistent with what little is known about the phase boundaries in this system^{24,27,28}, but also reveals new insights. In particular, we find several remarkable features. First, the ferromagnetic ansatz is seen to be indistinguishable from the exact ground state over a wide range of θ values, $\theta \leq -3\pi/4$ and $\theta \geq +\pi/2$, with sharp, possibly first order, transitions signalling vanishing of the ferromagnetic state at $\theta = \pi/2$ and $-3\pi/4$. Second, the ground state of the Heisenberg point at $\theta = 0$ is in the same correlator class as the AKLT state, supporting suggestions that there is a finite range of θ over which the ground state has the symmetry of the AKLT state²⁷. Third, although the indistinguishability for h_{ref} in the Haldane phase drops quickly as the dimerized phase is approached ($\theta \rightarrow -\pi/4$), the signature of the phase transition does not appear as strongly as the alternative Haldane to quadrupolar transition ($\theta \rightarrow +\pi/4$) for this system size.

Additionally, we have calculated the $n = N/2$ indistinguishability susceptibility, Eq. 12, for this model with $N = 36$ and $N = 72$ (Fig. 5). The sharp transitions from the ferromagnetic state are reflected in large peaks in the susceptibility; the height of these peaks is controlled only by the discretization of the θ values. These sharp peaks at $\theta = \pi/2$ and $-3\pi/4$ are consistent with the possibility of first order transitions out of the ferromagnetic phase. A well-pronounced transition also appears between the Haldane and the quadrupolar phase, with a pronounced shift due to finite size effects. The indistinguishability susceptibility is thus sensitive to the difference between first order and continuous phase transitions, with the latter showing finite size shifts due to the divergence of the intrinsic length scales.

We note that, in contrast to the clear signatures for transitions from the ferromagnetic phase and from the Haldane to quadrupolar phase, the transition from the dimerized phase to the Haldane phase is only very weak at these system sizes. A small peak does emerge at $N = 72$, but for $N = 36$ the peak corresponding to the transition appears considerably flattened out, almost to a plateau, and is also considerably shifted in location. To understand this behaviour, we analyzed the fully dimerized ansatz state derived at $\theta = -\pi/2$ with the omission of all even-bond terms in Eq. (13), as described above. Fig. 6 (b) shows that the indistinguishability for this ansatz state is relatively small, never exceeding 0.25, implying that this fully dimerized ansatz

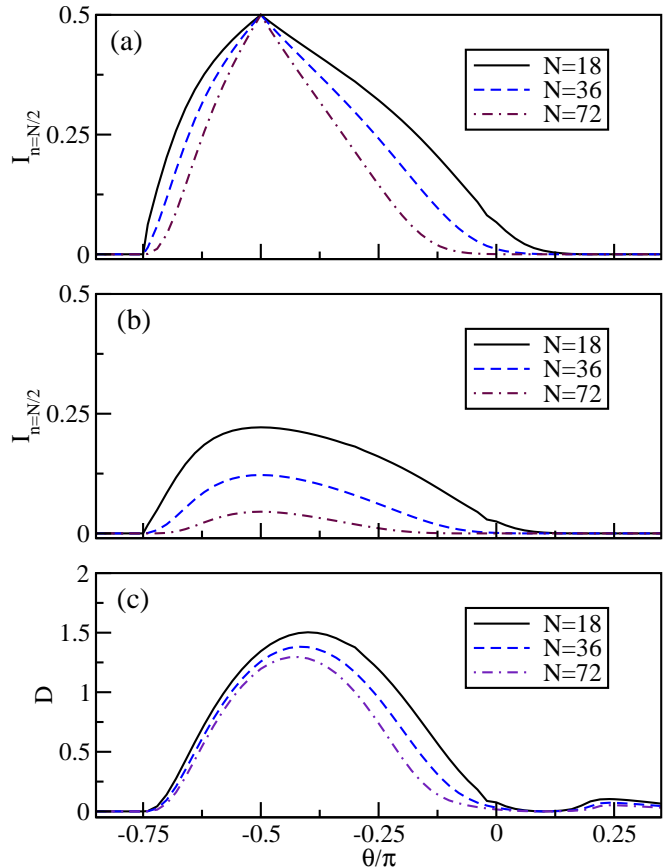


Figure 6: Analysis of the dimerized phase. (a) MPS ground state for $\theta = -\pi/2$ as the reference state. For small system sizes, the reference state remains a good ansatz state far beyond $\theta/\pi = -0.25$ into the Haldane regime. (b) $I_{N/2}$ for a strongly dimerized reference state obtained for $\theta = -\pi/2$ by omitting even-bond terms from the Hamiltonian, Eq. (13). The indistinguishability remains small even around the maximally dimerized point near $\theta/\pi = -0.5$, indicating that a product of dimers only poorly characterizes the system. (c) Dimerization order parameter (Eq. (14)) for three system sizes. The dimerization remains finite far towards the AKLT point, rendering the Haldane and dimerized phases hard to distinguish on small length scales.

only poorly describes the dimerized phase of Eq. (13), even in the proximity of the maximally dimerized point around $\theta/\pi = -0.5$. Our results thus confirm that there are strong fluctuations away from a simple state consisting entirely of products of dimers and that it is therefore difficult to precisely characterize the nature of the ground state in this parameter region.

To analyze the degree of dimerization we define a dimerization order parameter:

$$D = \frac{1}{N} \sum_{\text{bond } i} |H_i - H_{i+1}| \quad (14)$$

with $H_i = [\cos\theta(\mathbf{S}_i \mathbf{S}_{i+1}) + \sin\theta(\mathbf{S}_i \mathbf{S}_{i+1})^2]$. In these

units, the fully dimerized state is characterized by $D = 2.63$. We can then demonstrate the degree of dimerization by direct evaluation of Eq. 14. This is plotted in Fig. 6 (c), which shows a finite dimerization far into the Haldane regime. For the smallest system sizes, the dimerization order parameter vanishes only at the AKLT point. This is due to the explicit breaking of translational symmetry induced by our use of open boundary conditions as well as to our restricted system sizes. We therefore expect that the weak peak in the susceptibility at $N = 72$ should become more pronounced with larger system sizes or with periodic boundaries.

VII. CONCLUSION

Motivated by the importance of ansatz wavefunctions for developing physical insight into strongly correlated phases where the numerically obtained wave function may be available but too complex for physical analysis, we have introduced an indistinguishability measure I_n to assess the accuracy of ansatz functions by comparison with accurate numerical solutions. The indistinguishability measure quantifies the ability of any set of n -particle correlators to distinguish two states, with a value $I_n > 0$ in the thermodynamic limit showing that two states lie in the same correlator class and a value $I_n = 0$ indicating that they lie in different classes. The accuracy of an ansatz wavefunction can then be determined by evaluation of $I_n(A, E)$, the indistinguishability of the ansatz

state Ψ_A from the exact state Ψ_E . The real space scaling of the indistinguishability measure can be evaluated directly, or in terms of the quantum Chernoff bound²². We demonstrated with two one-dimensional examples, the well-known transverse Ising chain and a spin-1 bilinear-biquadratic chain, that this allows physically motivated ansatz wavefunctions to be matched to accurate numerical wavefunctions in different phases. We showed that the phase boundaries can be accurately obtained from the coincidence of $I_n(A, E)$ values for different ansatzes Ψ_A and further defined an indistinguishability susceptibility that characterizes the location of the quantum phase transition.

The indistinguishability measure I_n can be applied to analysis of ansatz wavefunctions using any of the many numerical techniques that are now available to efficiently obtain reduced density matrices, e.g., exact diagonalization, configuration interaction methods, density matrix renormalization group (DMRG)^{29,30} and tensor network methods (e.g., the projected entangled-pair state³¹, multi-scale entanglement renormalization ansatz³², etc.). As an example of a direct application, our measure may be used with exact diagonalization⁸ or DMRG^{33,34} to study ansatz fractional quantum Hall states.

We thank J. I. Korsbakken, A. Läuchli, S. Trebst and F. Verstraete for valuable discussions. We thank the NSF PIF and SNSF for support. Simulations were performed on the ETH Brutus cluster. While this manuscript was under review, we became aware of subsequent work³⁵ reporting related calculations for Ising chains.

-
- * Present Address: Physics Department, Virginia Tech, Blacksburg, Virginia 24061, USA
- ¹ X.-G. Wen, *Int. J. Mod. Phys B* **4**, 239 (1990).
 - ² F. Haldane, *Phys. Rev. Lett.* **51**, 605 (1983).
 - ³ S. Trugman and S. Kivelson, *Phys. Rev. B* **31**, 5280 (1985).
 - ⁴ J. Jain, *Composite Fermions* (Cambridge University Press, 2007).
 - ⁵ I. Affleck et al., *Phys. Rev. Lett.* **59**, 799 (1987).
 - ⁶ A. Kitaev, *Ann. Phys.* **303**, 2 (2003).
 - ⁷ R. Laughlin, *Phys. Rev. Lett.* **50**, 1395 (1983).
 - ⁸ R. Morf, *Phys. Rev. Lett.* **80**, 1505 (1998).
 - ⁹ C. Helstrom, *Quantum Detection and Estimation Theory* (Academic, 1976).
 - ¹⁰ C. Fuchs and J. van de Graaf, *IEEE Trans. Inf. Theory* **45**, 1216 (1999).
 - ¹¹ J. I. Korsbakken et al., *Phys. Rev. A* **75**, 042106 (2007).
 - ¹² G. Vidal, *Phys. Rev. Lett.* **91**, 147902 (2003).
 - ¹³ A. J. Daley, C. Kollath, U. Schollwöck, and G. Vidal, *Journal of Statistical Mechanics: Theory and Experiment* **2004**, P04005 (2004).
 - ¹⁴ S. Östlund and S. Rommer, *Phys. Rev. Lett.* **75**, 3537 (1995).
 - ¹⁵ F. Verstraete, J. I. Cirac, and V. Murg, *Adv. Phys.* **57**, 143 (2008).
 - ¹⁶ S. Furukawa et al., *Phys. Rev. Lett.* **96**, 047211 (2006).
 - ¹⁷ T. Osborne and M. Nielsen, *Phys. Rev. A* **66**, 032110 (2002).
 - ¹⁸ A. Osterloh et al., *Nature* **416**, 608 (2002).
 - ¹⁹ G. Vidal et al., *Phys. Rev. Lett.* **90**, 227902 (2003).
 - ²⁰ P. Zanardi and N. Paunkovic, *Phys. Rev. E* **74**, 031123 (2006).
 - ²¹ H. Zhou and J. Barjaktarevic, *J. Phys. A* **41**, 412001 (2008).
 - ²² K. Audenaert et al., *Phys. Rev. Lett.* **98**, 160501 (2007).
 - ²³ S. Sachdev, *Quantum Phase Transitions* (Cambridge University Press, Cambridge, England, 1999).
 - ²⁴ A. Läuchli et al., *Phys. Rev. B* **74**, 144426 (2006).
 - ²⁵ I. Affleck, T. Kennedy, E. Lieb, and H. Tasaki, *Commun. Math. Phys.* **115**, 477 (1988).
 - ²⁶ D. Arovav et al., *Phys. Rev. Lett.* **60**, 531 (1998).
 - ²⁷ S. Girvin and D. Arovav, *Phys. Scr.* **T27**, 156 (1989).
 - ²⁸ J. Sólyom, *Phys. Rev. B* **36**, 8642 (1987).
 - ²⁹ S. White, *Phys. Rev. Lett.* **69**, 2863 (1992).
 - ³⁰ U. Schollwöck, *Rev. Mod. Phys.* **77**, 259 (2005).
 - ³¹ F. Verstraete and J. I. Cirac, *cond-mat/0407066*.
 - ³² G. Vidal, *Phys. Rev. Lett.* **99**, 220405 (2007).
 - ³³ N. Shibata and D. Yoshioka, *Phys. Rev. Lett.* **86**, 5755 (2001).
 - ³⁴ A. Feiguin et al., *Phys. Rev. Lett.* **100**, 166803 (2008).
 - ³⁵ C. Invernizzi and M. Paris, *arxiv:0905.0980* (2009).